Human Serum Albumin in the presence of Small Platinum Nanoparticles

Xiaomin Yang, Erika Porcel, Laurent Marichal, Cesar Gonzalez Vargas, Amine Khitous, Daniela Salado-Leza, Xue Li, Jean-Philippe Renault, Serge Pin, Hynd Remita, et al.

Title

Platinum Nanoparticles Stabilize Human Serum Albumin Structure

Xiaomin Yang[1], Erika Porcel[1], Laurent Marichal[2], Cesar Gonzalez Vargas[1], Amine Khitous[1], Daniela Salado-Leza[1,3], Xue Li[1], Jean-Philippe Renault[2], Serge Pin[2], Hynd Remita[4], Frank Wien[5#], Sandrine Lacombe[1#]

[1]Université Paris-Saclay, CNRS, Institut des Sciences Moléculaires d'Orsay, 91405 Orsay, France

[2]Université Paris-Saclay, CEA, CNRS, NIMBE, 91191, Gif-sur-Yvette, France.

[3]CONACyT, Faculty of Chemical Sciences, Autonomous University of San Luis Potosi, 78210 San Luis Potosi, Mexico

[4]Université Paris-Saclay, CNRS, Institut de Chimie Physique, UMR 8000, 91405 Orsay, France

[5]Université Paris-Saclay, Synchrotron Soleil, 91190, Saint-Aubin, France

Corresponding Author:

Prof. Sandrine Lacombe

Université Paris-Saclay, CNRS, Institut des Sciences Moléculaires d'Orsay, 91405, Orsay, France; Tel: +33 (1) 6915 8263 ; E-mail: sandrine.lacombe@u-psud.fr.

Prof. Frank Wien

Université Paris-Saclay, Synchrotron Soleil, 91190, Saint-Aubin, France; Tel: +33 (1) 6935 9665 ; E-mail: frank.wien@synchrotron-soleil.fr.

Abstract

Noble metals, especially platinum nanoparticles (Pt NPs) have immense potential in nanomedicine as therapeutic agents on account of their high surface area, intrinsic

catalytic properties, etc. However, our understanding of the interaction of nanoparticles with biological entities, especially proteins, is far behind the explosive development of nanotechnology. In this study, we measure the structural and stability changes of proteins at nanomolar concentrations upon interaction with Pt NPs using various techniques. A large increase of 18°C in the thermal unfolding of human serum albumin (HSA) with Pt NPs at the molar ratio 1:1 is observed using synchrotron radiation circular dichroism (SRCD), due to Pt NPs increased thermal stability of HSA through preferential hydration processes. The use of SRCD allows measuring critical parameters on NPs-protein interactions, provides additional information for understanding the influential role of PEG coating in NPs-cell interaction and has implications for nanomedicine and nanotoxicology.

Key words: Pt NPs, HSA, synchrotron radiation circular dichroism, thermal stability, thermodynamic properties

1. Introduction

After the pioneering work of Rosenberg in 1965, cis-platin have been widely used in cancer therapy (Rosenberg et al., 1969). From then on, numerous new Pt compounds have been discovered with better therapeutic performances than cis-platin (Dasari and Tchounwou, 2014). Despite of the clinical success of the Pt complex, it suffers from a lack of tumor tissue selectivity leading to some severe side effects (Medhat et al., 2017). Advances in nanotechnology have provided new and powerful tools in the development of multifunctional Pt NPs for effective detection and treatment of cancer, overcoming limitations associated with conventional cancer diagnosis and therapy (Srinivasan et al., 2015). Radiolytic synthesis (by gamma rays, X-rays, electron beams or other types of ionizing radiation) provides a major advantage for a large-scale production of monodisperse particles as it generates a uniform distribution of reducing agents in the

entire solution during the irradiation process (Abidi et al., 2010; Belloni et al., 1998; Holade et al., 2017; Uttayarat et al., 2015). Another advantage is that these nanoparticles are freshly prepared in water without using potentially toxic solvents. The functionalization of the NPs can be achieved during the radiolytic synthesis by adding an appropriate substance to the reaction (Freitas de Freitas et al., 2018). The functionalization with ligands or polymers such as poly(ethylene) glycol PEG enhances the stability and control of their size (Wang et al., 2011).

Pt NPs have received considerable attention in nanomedicine due to their tunable, highly sensitive optical, catalytic, and therapeutic properties. A promising area of research involves the amplification of radiotherapy in the presence of Pt NPs at the tumor site (Lacombe et al., 2017). The properties of radioenhancement were demonstrated for Pt NPs at nanoscale (Porcel et al., 2010; Schlathölter et al., 2016) and at cellular level (KA et al., 2018; Salado-Leza et al., 2020; Yang et al., 2020c). For this use, intravenous administration of NPs is preferable than intra tumoral, to avoid pain to the patient and ensure reproducible distribution via enhanced permeability and retention effect (EPR). Thus, further exploration of the interaction of NPs with biological systems and blood proteins in particular is an important issue.

Proteins participate in most of the biological functions of the living matter and play a crucial role in its maintenance. Their biologic activity highly depends on their three-dimensional secondary structure (Takano et al., 2016), while undesirable interactions with NPs, may lead to protein aggregation or disfunction (Saptarshi et al., 2013). The present study is focused on the interaction of Pt NPs with human serum albumin (HSA), since serum albumins are major circulatory proteins, which play crucial roles in many important physiological functions like maintaining plasma oncotic pressure, transporting cargo, antioxidant and enzymatic activities (Lee and Wu, 2015). Once NPs

enter systemic circulation, particle-protein interaction is the first phenomenon taking place before distribution into various organs (Mu et al., 2014). The impact of NPs, when they interact with blood proteins, is thus a major question to answer. In particular, a modification of the protein structure is expected to be dramatic, by changing physiological functions (Prasanth et al., 2018).

The analysis of the structure and stability of proteins in protein-Pt NPs is a key to investigate and understand the change of the proteins' properties after their interaction with Pt NPs. The structure analysis can be performed with various techniques. Among them, Circular Dichroism (CD) allows to characterize the secondary structure, and thus folding properties of proteins, and has recently been used to detect structure changes of proteins interacting with NPs (Micsonai et al., 2015). Synchrotron Radiation Circular Dichroism (SRCD) spectroscopy is superior to the conventional CD spectroscopy, thanks to the high intensity of photon emission, and the higher signal-to-noise levels of the CD spectra. This allows to use lower amounts of proteins, and to observe subtle conformational changes as shown by Wallace and Janes (Wallace and Janes, 2010). Additionally, the spectral range in SRCD extends down to 175 nm (compared to 190 nm in CD). This enables elucidating finer details in the secondary structure of proteins (Gobeaux and Wien, 2018), especially in the presence of nanoparticles (Sanchez-Guzman et al., 2020). SRCD allowed Laera et al. to discover that the thermal unfolding temperature of HSA decreased by 6ºC upon interaction with silver NPs. This indicates that the HSA is significantly destabilized by the NPs, possibly due to a more flexible folded structure formed in the presence of the silver NPs (Laera et al., 2011). On the contrary, Robin Capomaccio et al finds a melting temperature (T_m) of 69ºC for free HSA and of 75.4 ℃ for the AuNP-HSA complexes using SRCD, suggesting that Au NPs stabilize HSA, both by increasing its thermal stability, and by reducing its

propensity to aggregate (Capomaccio et al., 2015). Recently, our group has shown that Gd NPs (AGuIX) can modify the stability of HSA due to an indirect interaction (Yang et al., 2020a).

In this study, Pt NPs were synthesized, characterized and their potential impact on HSA was investigated. Our aim was to understand the interaction between Pt NPs and serum blood proteins by complementary techniques, an area in which the number of available reports is limited. In particular, we measured the secondary structure of proteins in low nanomolar concentrations, and in particular, the structural and thermal stability changes associated with proteins to Pt NPs up to 1:1 particle ratios using the SRCD technique at DISCO, Synchrotron SOLEIL. This extremely sensitive technique has allowed us to show that Pt NPs have significantly increased the thermal stability of HSA, and has also allowed accessing new detailed information about NPs-protein interactions.

2. Experimental

2.1. Materials and chemicals

Tetraammine platinum (II) chloride salt $[Pt(NH_3)_4]Cl_2 \cdot H_2O$ (Sigma-Aldrich, USA), poly(ethylene glycol) ($H(OCH_2CH_2)nOH$, M_W= 1000 $g.mol^{-1}$, Fluka), potassium phosphate monobasic (KH_2PO_4), sodium phosphate dibasic (Na_2HPO_4), HSA was purchased from Sigma-Aldrich, USA. HSA samples were prepared by dissolving HSA powder in 10 mM phosphate buffer at pH 7.0. All chemicals were of analytical grade. Pure water used in all experiments was filtered (18.4 MΩ cm) by a Milli-Q system (Millipore, Milford, MA, USA).

2.2. Synthesis of Pt NPs

Pt NPs were synthesized by facile and ecofriendly one-step radiolysis. The procedure of synthesis and characteristics of these NPs are detailed in the French Patent

Application: Nanoparticules et procédé de preparation, FR1900008 (Salado-Leza et al., 2020; Yang et al., 2020b). Briefly, the reduction was achieved in aqueous solution using $Pt(NH_3)_4Cl_2$ (10^{-2} mol/L) as precursor and polyethylene glycol (PEG-OH 1000, 1 mol/L) as radical scavenger, stabilizer and biocompatible capping agent. After thorough deaeration with flushing nitrogen gas, the solutions were irradiated by a γ-source provided by a panoramic ^{60}Co γ-facility (E= 1.33 MeV, LET= 0.2 keV.μm-1) with dose rate of 68.2 $Gy.min^{-1}$. Pt^{II} was completely reduced to Pt^0 at a dose of 1,000 Gy (Porcel et al., 2012; Porcel et al., 2010). The obtained Pt NPs were lyophilized for storage at 4 ºC for months.

2.3. Characterization of Pt NPs

Morphological characterization was conducted by a TEM-STEM JEOL1400 (Ernest) transmission electron microscopy (TEM) with an accelerating voltage of 120 kV. For TEM observations, a drop of the Pt NPs solution was deposited onto copper grids (200 mesh, Agar Scientific Ltd). The grids were dried under a flow of N_2under ambient conditions before observations. Statistical analysis of Pt NPs diameter was converted to cumulative number-based distributions with 'Image J' program.

Electrokinetic properties (ζ–potential) of Pt NPs were measured with ζ–potential analyzer model Zeta Potential WALLIS (Cordouan Technologies, France). Pt NPs were diluted in Mili-Q water to reach 0.1 mM, and measured at 25ºC in a disposable folded capillary cell.

The optical absorption measurements were performed on a CARY 300 Scan UV-Visible Spectrophotometer (Int. Agilent) in the frequency range of 200 nm-800 nm at room temperature before and after irradiation. The as-synthesized Pt NPs were diluted with Milli-Q water to a final concentration of Pt [1 mM] for UV–visible absorption measurements.

150 **2.4. Preparation of the samples**

151 The HSA mother solution (20 mg/mL) was prepared by dissolving HSA powder in 10
152 mM phosphate buffer at pH 7.4 (Shaw and Pal, 2008). The concentration of HSA was
153 determined by absorbance measurements using molar extinction coefficients of 0,58
154 $(g/L)^{-1}cm^{-1}$ at 280 nm (Dockal et al., 1999).

155 Pt NPs-HSA samples at different Pt NPs/HSA molar ratios (1:30 to 1:1) were
156 prepared by mixing a 15 μM HSA solution with different concentrations of Pt NPs in
157 phosphate buffer at pH 7.0. The samples were incubated at room temperature for 40
158 minutes before measurements.

159 **2.5. Dynamic light scattering**

160 The hydrodynamic diameter of Pt NPs in the absence and presence of proteins (15 μM)
161 (with molar ratios of Pt NPs/HSA from 1:30 to 1:1) was measured by dynamic light
162 scattering (DLS) using a Cordouan VASCO-2 particle size analyzer (Cordouan
163 Technologies, France). The Pt NPs were diluted in Mili-Q water to a final concentration
164 of 0.5 mM, and the measurements were conducted at 25ºC in a semi-micro polystyrene
165 (PS) cuvette.

166 **2.6. Isothermal Titration Calorimetry (ITC)**

167 Adsorption isotherms of HSA on Pt NPs were performed by calorimetry using a
168 MicroCal PEAQ-ITC (Malvern). All the solutions were thoroughly degassed prior to the
169 titrations to avoid the formation of bubbles in the calorimeter cell. The reaction cell
170 (280 μL) was loaded with a HSA solution at 1×10^{-4} mol/L. The syringe (75 μL) was
171 filled with a Pt NPs solution at 2×10^{-3} mol/L. The proteins and NPs were prepared in
172 the same phosphate buffer (pH 7.4) to prevent any pH effect. The experiments were
173 done in duplicate at 20 °C by adding 2.4 μL of the Pt NPs solution to the HSA solution
174 with an equilibration interval of 200 s. Raw data were obtained as a plot of heat (μcal)

against the injection number, and featured a series of peaks for each injection. These raw data peaks were transformed using the instrument software to obtain a plot of the enthalpy change per mole of injectant (ΔH^0, kcal·mol^{-1}) against the molar ratio. Control experiments included the titration of the Pt NPs solution into buffer, buffer into HSA, and buffer into buffer, with the same used sample concentration. Corrected data refer to experimental data after subtraction of the control data.

2.7. Synchrotron radiation circular dichroism (SRCD)

SRCD spectra acquisition

The SRCD spectra of samples were measured on the DISCO beamline, SOLEIL synchrotron radiation facility, Saint-Aubin, France.

Prior to the measurement, the instrument was calibrated using an aqueous solution of (+) camphorsulphonic acid (CSA). To prepare the sample, 4 μL Pt NPs–HSA solution was placed in CaF_2 cuvettes with a 50 μm pathlength (Wien and Wallace, 2005).

The HSA spectra were collected between 170 and 261 nm with a step size of 1 nm and an integration time of 1200 ms/nm at 37ºC. All the spectra were recorded in triplicate, averaged, baseline subtracted and zeroed using CDToolX software (Lees et al., 2004). Raw data ellipticity expressed in millidegrees (mdeg) was converted to molar circular dichroism values (Δε). For the molar circular dichroism values (Δε, $M^{-1}.cm^{-1}$ = $L.mol^{-1}.cm^{-1}$), the following Eq. 1 was applied:

$$\Delta\varepsilon = \theta \times \frac{(0.1 \times \mathrm{MRW})}{(P \times C) \times 3298} \quad (1)$$

where the MRW (mean residue weight) of HSA is 113.8 Da ($g.mol^{-1}$), P (pathlength) is 0.005 cm (measured by interferometry) and C (protein concentration) was ~1 mg/mL.

Thermal denaturation

Thermal denaturation studies were carried out by collecting SRCD spectra in a temperature range between 26 and 95°C with a step of 3°C. Three spectra were recorded with 5 minutes equilibration time for each temperature.

Ellipticity values were obtained from thermal denaturation curves for each of the three peaks (223 nm, 210 nm and 192 nm) at each temperature. They were normalized by setting the peak values at 26°C to 1.0. The decreasing of the relative intensity of protein with temperature has been fitted to a Boltzmann type equation Eq. 2 with the software OriginLab (Laera et al., 2011).

$$y = A + \frac{\mathrm{B-A}}{1+e^{\frac{x-x_0}{dx}}} \quad (2)$$

(where X is the temperature, X_0 the melting temperature (T_m), and dx the width of the thermal transition) for a simple two-state unfolding process. T_m of the protein defined as the midpoint of the unfolding transition.

Structure analysis

The contents of α-helix, β-sheet, turn and other structures of HSA were calculated from SRCD spectra using BeStSel, a web server used for accurate secondary structure components determination (Micsonai et al., 2018; Micsonai et al., 2015).

3. Results and discussions

3.1. Synthesis and characterization of Pt NPs

The Pt NPs synthesized in water by radiolysis were precisely characterized using DLS, TEM and the zeta potential technique (**Figure 1**).

The Pt NPs observed by TEM show semi-spherical morphologies (**Figure 1a**) and a uniform size distribution with an average metallic core diameter of 3.0±0.8 nm (**Figure 1b**). DLS measurements showed that Pt NPs have an average hydrodynamic diameter of 18±2.6 nm (**Figure 1c**). Significant differences between TEM analysis and DLS measurement indicate the Pt NPs PEG coating. The zeta potential value of Pt NPs in MiliQ water is -14.2±4.1 mV. This result is in good agreement with experimental results of other works (Ehi-Eromosele, 2016; Ibrahim et al., 2016), the PEG coated NPs have an average negative ζ–potential of -14 mV and -17 mV, respectively, in water (pH 6~7), which leads to interparticle repulsion (Ehi-Eromosele, 2016).

[**Figure 1**]

The reduction of Pt complex and the formation of Pt NPs were monitored using UV-vis absorption spectroscopy. Metallic NPs display strong optical absorptions due to their surface plasmon resonance (SPR). Platinum nanoparticles have a plasmon in the UV range (Salado-Leza et al., 2019; Yang et al., 2020b). **Figure 2** shows the UV-vis spectra of the aqueous solutions containing $[Pt(NH_3)_4]Cl_2$ and PEG-OH before and after irradiation.

The spectra reveal that, before irradiation, the aqueous solutions composed of $[Pt(NH_3)_4]Cl_2$ or $[Pt(NH_3)_4]Cl_2$ in the presence of PEG-OH, have the absorbance of the main peak close to 240 nm and a small shoulder around 290 nm, which correspond to the ligand-to-metal charge transfer (LMCT) band between $(NH_3)_4^{2+}$ and Pt^{II} ions (Gharibshahi and Saion, 2012). After irradiation, the two initial absorption peaks disappear due to the complete reduction of Pt^{II} into Pt^0 leading to formation of Pt NPs. Thus, there was no further charge transfer possible from ligand to metal ions (Inwati et al., 2016). Moreover, the appearance of a surface plasmon absorption band with a single

broad peak centered at around 270 nm indicated the presence of Pt NPs (Moores and Goettmann, 2006; Yang et al., 2020b).

The inserted picture in **Figure 2** shows the color of the colloidal solution, which changed from colorless (before irradiation) to dark brown (after gamma irradiation). The colour change is due to the radiolytic reduction of $[Pt(NH_3)_4]^{2+}$ ions to Pt^0 atoms indicating the formation of colloidal Pt NPs (Gharibshahi and Saion, 2012; Salado-Leza et al., 2020) as mentioned before.

[**Figure 2**]

3.2. Dynamic light scattering analysis

In the present work, DLS was used to measure the hydrodynamic diameter of different concentrations of Pt NPs in the absence and presence of HSA at pH 7.4 in 10 mmol/L phosphate buffer. No significant change in the NPs size distribution after exposure to HSA at room temperature. It demonstrated there was no complex formation, which is probably due to the grafting of hydrophilic PEG-OH on Pt NPs having a high capacity to prevent the adsorption of proteins (Pelaz et al., 2015; Wang et al., 2015). Furthermore, PEGylation might prevents the uptake of Pt NPs by Reticuloendothelial System (RES) and enhance the circulation lifetime of NPs inside the body (Suk et al., 2016).

[**Figure 3**]

3.3. Isothermal Titration Calorimetry

The binding properties of the Pt NPs with HSA were consecutively studied using ITC. **Figure 4a** and **Figure 4b** show the plot of enthalpy change (ΔH^0) against Pt NPs-HSA molar ratio. The amount of heat due to the controls (dilution) is measured and subtracted from the amount of the heat obtained for the Pt NPs-protein system. ITC results did not show any significant binding, and no thermodynamic parameters could

be obtained. This finding is consistent with previous studies on telodendrimer-based NPs having PEG in the surface (Li et al., 2012). Indeed, the functionalization of NPs by PEG prevents interactions with proteins (Gref et al., 2000).

[**Figure 4**]

3.4. Synchrotron radiation circular dichroism (SRCD)

SRCD spectra acquisition

The adsorption of proteins on the surface of nanomaterials, may induce conformational changes for some proteins, which influence the functionality and biological activity of the proteins (Satzer et al., 2016; Shemetov et al., 2012). The SRCD spectroscopy is widely used to study the conformation of proteins in aqueous solution. The far UV SRCD spectra (170~261 nm) provide the variations in the secondary structure of proteins as a result of the molecular interactions with other materials (Prasanth et al., 2018). **Figure 5** shows the SRCD spectra of pure HSA and HSA in the presence of different concentrations of Pt NPs (0.5 mM, 1 mM, 2 mM, and 15 mM), corresponding to Pt NPs-HSA ratios of 1:30, 1:15, 1:7.5, and 1:1. The spectrum exhibits two negative bands at 210 and 223 nm, one positive band at 192 nm, characteristic of the α-helical structure. The negative peak at 223 nm is due to the n→π* transition of the carbonyl group of peptide, while the parallel and perpendicular excitation of the peptide π → π * transition is responsible for the other negative peak at 210 nm and the positive peak at 192 nm (Gobeaux and Wien, 2018).

With the addition of different amounts of Pt NPs to the HSA aqueous solution, the SRCD spectra of the Pt NPs-HSA mixture remained unchanged for three repeated scans

291 at 37°C (**Figure 5**). This clearly indicates that Pt NPs does not induce a significant
292 conformation change of the protein at 37°C.

293 [**Figure 5**]

294 **Thermal denaturation**

295 The thermal stability of proteins without or with Pt NPs was assessed by recording
296 the intensity of SRCD signal at 192 nm as a function of temperature. SRCD spectra of
297 pure HSA and Pt NPs-HSA at different ratios from 1:30 to 1:1 were recorded at
298 temperatures in the range of 26~95°C. The temperature scans of Pt NPs:HSA=1:7.5 are
299 presented in **Figure 6**. The spectra clearly indicate that the temperature increase causes
300 a gradual decrease of the alpha helical profile.

301 [**Figure 6**]

302 The decreasing of the relative intensity of protein with temperature in **Figure 7**,
303 showed that the thermal denaturation curves were shifted with the increasing ratio of Pt
304 NPs-HSA towards higher T_m. The resulting T_m is reported in **Table 1**. From the results,
305 we observe the T_m increases with increasing the Pt NPs concentration. The free HSA
306 has a T_m of 56°C, which is in good agreement with reported results that HSA undergoes
307 morphological changes at 56°C (Das et al., 2014). The T_m of Pt NPs-HSA=1:1 is 74°C,
308 increased 18°C compared to the T_m of free HSA. The tremendous increase in T_m
309 suggests that Pt NPs increase the thermal stability of HSA. It was shown by other
310 groups that silver NPs decrease the thermal stability of HSA, while gold NPs (using the
311 same preparation method as silver NPs) did not significantly change it (Laera et al.,
312 2011) even at same ratio of NPs-HSA. However, different experimental conditions must
313 be taken into consideration.

314 **Structure analysis**

315 A more detailed analysis of the two spectra using deconvolution software BeStSel
316 allows estimating the percentage of secondary structure α-helix, *β*-sheet, turn and
317 random coil elements present in each SRCD spectrum.

318 **Figure 7** shows that the content of *α*-helix conformation of HSA decreases from 61%
319 to 29%, on contrary *β*-sheet and random coil increase from 1% to 20% and 30% to 40%
320 respectively, with a subsequent increase of unfolded protein, as a function of the
321 increasing temperature. The turn component of HSA remains practically constant for all
322 the samples ~10% (in the interval 26~95°C). The same trends were found in the
323 presence of Pt NPs, except the structuration in beta sheet was significantly lower at high
324 temperature with the addition of Pt NPs (ratios of Pt NPs-HSA ranging from 1:30 to
325 1:1).

326 Protein conformational compositions in pure HSA indicate an increase in *β*-sheet
327 conformation from 0% to 20% at the expenses of the α-helix content (which diminished
328 from 57% to 28%) when the temperature rises from 38°C to 89°C. As the temperature
329 increases, the cooperative hydrogen bonds that stabilized the helical structure weakened
330 and expose hydrophobic groups to the solvent, partially unfolding the protein structure,
331 which favours the formation of beta-sheet-rich amyloid fibrils (Juárez et al., 2009). It
332 was shown that the presence of NPs can influence the protein fibrillation process
333 (Mahmoudi et al., 2013). In this case, the alpha helix decreased less in the presence of
334 Pt NPs than in pure HAS, and an increase in random coils substituted the α-helix loss,
335 indicating that Pt NPs prevent inter-protein interactions, and thus increase the
336 conformational stability of proteins.

343 [**Figure 7**]

344 **Thermodynamic analysis**

The biological responses to NPs are influenced by the forces (such as electrostatic, hydrophobic or Van der Waals forces) present at the bio-nano interface (Mariam et al., 2017). Hence it is essential to have a complete understanding of the thermodynamics of Pt NPs-HSA interaction. The thermodynamic properties (enthalpy variation, entropy variation) obtained by fitting the temperature changes of local helix content to the Van't Hoff equation Eq. 3 (Greenfield, 2006):

$$lnK = \frac{-\Delta H^\circ}{RT} + \frac{\Delta S^\circ}{R} \quad (3)$$

where K is the binding constant at the corresponding temperature, and R is universal gas constant. ΔH^0 and ΔS^0 are presented in **Table 1**. We found out a gradual increase of enthalpy variation and entropy variation in the presence of Pt NPs with increasing T_m. It can be seen that the enthalpy variation increases significantly from 87 kJ/mol of pure HSA to 116 kJ/mol of Pt NPs-HSA=1:1. The same phenomenon was observed by other groups. It was explained by Senske *et al*, that nanoparticles can stabilize the native conformation of proteins compared to the unfolded state under external stresses such as temperatures (Senske et al., 2014). This stabilization is explained by an unfavourable interaction of the protein and the nanoparticles leading to a preferential exclusion of the nanoparticles from the protein surface and a preferential hydration of the protein. Since the solvent accessible surface area is usually increased for the unfolded state, in the presence of Pt NPs, this would increase the thermodynamically unfavourable situation and require more energy for unfolding (unfolding enthalpy variation would increase with the Pt NPs concentration) than in water. As a result, the folding equilibrium should tend to shifted toward the more folded, native state.

Finally, the assumption of the increase of the HSA stability with Pt NPs was supported by good agreement with the thermodynamic data and structure analysis for the thermal unfolding transition determined by far-UV SRCD.

[**Figure 8**]

4. Conclusion

In summary, we have successfully synthesized Pt NPs with homogeneous size using radiolytic reduction method by gamma irradiation. The DLS and TEM images indicate that the synthesized Pt NPs are semi-spherical in shape and uniform in size. UV-Vis spectra suggest the complete reduction of Pt^{II} and the formation of Pt NPs. The coherent results of hydrodynamic diameter and ITC demonstrated that Pt NPs do not bind to HSA even at the high ratio of 1 Pt NP per HSA. SRCD secondary spectra show that even the high concentrations of Pt NPs do not induce significant change of the protein conformation. The thermal stability of protein is assessed by SRCD by monitoring the spectral changes in the spectra with increasing temperature. More importantly, an increase of 18℃ in the thermal unfolding of HSA upon interaction with Pt NPs was found, which support the fact that Pt NPs stabilize the HSA structure. This structure analysis showed that, as the temperature rises, the loss of α-helical content of HSA was decreased whereas a significant reduction in β-sheet was observed. This is due to increased stability of HSA in the presence of Pt NPs. The modification of the protein stability can be attributed to the preferential hydration of the protein. This stabilizing effect renders Pt NPs highly promising and applicable to be used as biocompatible stabilizing agents for proteins.

Author contribution

X.Y. synthesized and characterized Pt NPs, performed and analysed the DLS, UV-Vis spectroscopy, carried out the SRCD spectra analysis, data interpretation and drafted the manuscript. E.P. supervised the experimental protocols. L.M., S.P., J.P.R., A.K. conceived and performed the experiments of ITC. D.S.L, C. G., A. K. and X.L. contributed to the paper modifications. F.W., X. Y., E. P., A.K., C. G. optimized and

performed the SRCD experiments. H.R., and D.S.L were engaged in nanoparticles design, synthesis and characterization. S.L. conceived the entire project, reviewing and editing the manuscript. All authors revised the manuscript.

Acknowledgements

X.Y. acknowledges support from China scholarship council (CSC, N° 201607040068). We acknowledge support from the Université Paris Saclay for the "Inititative de Recherche Stratégique" IRS NanoTheRad project. This work also benefited from the RESPORE grant. SRCD measurements on DISCO beamline at SOLEIL synchrotron light source were performed under the proposal 20171494. We thank Ruxandra Gref (Institut des Sciences Moléculaires d'Orsay, Université Paris Saclay) for providing kind help on ITC experiments.

Reference

Abidi, W., Selvakannan, P., Guillet, Y., Lampre, I., Beaunier, P., Pansu, B., Palpant, B., Remita, H., 2010. One-pot radiolytic synthesis of gold nanorods and their optical properties. The Journal of Physical Chemistry C 114, 14794-14803.

Belloni, J., Mostafavi, M., Remita, H., Marignier, J.-L., Delcourt, M.-O., 1998. Radiation-induced synthesis of mono-and multi-metallic clusters and nanocolloids. New Journal of Chemistry 22, 1239-1255.

Capomaccio, R., Jimenez, I.O., Colpo, P., Gilliland, D., Ceccone, G., Rossi, F., Calzolai, L., 2015. Determination of the structure and morphology of gold nanoparticle–HSA protein complexes. Nanoscale 7, 17653-17657.

Das, N.K., Ghosh, N., Kale, A.P., Mondal, R., Anand, U., Ghosh, S., Tiwari, V.K., Kapur, M., Mukherjee, S., 2014. Temperature induced morphological transitions from native to unfolded aggregated states of human serum albumin. The Journal of Physical Chemistry B 118, 7267-7276.

Dasari, S., Tchounwou, P.B., 2014. Cisplatin in cancer therapy: molecular mechanisms of action. European journal of pharmacology 740, 364-378.

Dockal, M., Carter, D.C., Rüker, F., 1999. The three recombinant domains of human serum albumin structural characterization and ligand binding properties. Journal of Biological Chemistry 274, 29303-29310.

Ehi-Eromosele, C., 2016. The Effect of Polyethylene Glycol (PEG) Coating on the Magneto-Structural Properties and Colloidal Stability Of Co0. 8Mg0. 2Fe2O4 Nanoparticles for Potential Biomedical Applications. Digest Journal of Nanomaterials and Biostructures.

Freitas de Freitas, L., Varca, G., dos Santos Batista, J., Benévolo Lugão, A., 2018. An Overview of the Synthesis of Gold Nanoparticles Using Radiation Technologies. Nanomaterials-Basel 8, 939.

Gharibshahi, E., Saion, E., 2012. Influence of dose on particle size and optical properties of colloidal platinum nanoparticles. International journal of molecular sciences 13, 14723-14741.

Gobeaux, F., Wien, F., 2018. Reversible assembly of a drug peptide into amyloid fibrils: a dynamic circular dichroism study. Langmuir 34, 7180-7191.

Greenfield, N.J., 2006. Using circular dichroism collected as a function of temperature to determine the thermodynamics of protein unfolding and binding interactions. Nature protocols 1, 2527.

Gref, R., Lück, M., Quellec, P., Marchand, M., Dellacherie, E., Harnisch, S., Blunk, T., Müller, R., 2000. 'Stealth'corona-core nanoparticles surface modified by polyethylene glycol (PEG): influences of the corona (PEG chain length and surface density) and of the core composition on phagocytic uptake and plasma protein adsorption. Colloids and Surfaces B: Biointerfaces 18, 301-313.

Holade, Y., Servat, K., Tingry, S., Napporn, T.W., Remita, H., Cornu, D., Kokoh, K.B., 2017. Advances in electrocatalysis for energy conversion and synthesis of organic molecules. ChemPhysChem 18, 2573-2605.

Ibrahim, I.M., Abbas, A.K., Naser, D.K., 2016. SYNTHESIS AND ZETA POTENTIAL OF NOBLE METALS (Pt, Au, Ag AND Cu) NANOPARTICLES PREPARED BY PULSE LASER ABLATION. Science International 28.

Inwati, G.K., Rao, Y., Singh, M., 2016. In situ free radical growth mechanism of platinum nanoparticles by microwave irradiation and electrocatalytic properties. Nanoscale research letters 11, 458.

Juárez, J., Taboada, P., Mosquera, V., 2009. Existence of different structural intermediates on the fibrillation pathway of human serum albumin. Biophysical journal 96, 2353-2370.

KA, M.A., Ab Rashid, R., Lazim, R.M., Dollah, N., Razak, K.A., Rahman, W., 2018. Evaluation of radiosensitization effects by platinum nanodendrites for 6 MV photon beam radiotherapy. Radiation Physics and Chemistry 150, 40-45.

Lacombe, S., Porcel, E., Scifoni, E., 2017. Particle therapy and nanomedicine: state of art and research perspectives. Cancer nanotechnology 8, 9.

Laera, S., Ceccone, G., Rossi, F., Gilliland, D., Hussain, R., Siligardi, G., Calzolai, L., 2011. Measuring protein structure and stability of protein–nanoparticle systems with synchrotron radiation circular dichroism. Nano letters 11, 4480-4484.

Lee, P., Wu, X., 2015. Modifications of human serum albumin and their binding effect. Current pharmaceutical design 21, 1862-1865.

Lees, J., Smith, B., Wien, F., Miles, A., Wallace, B., 2004. CDtool—an integrated software package for circular dichroism spectroscopic data processing, analysis, and archiving. Analytical biochemistry 332, 285-289.

Li, Y., Budamagunta, M.S., Luo, J., Xiao, W., Voss, J.C., Lam, K.S., 2012. Probing of the assembly structure and dynamics within nanoparticles during interaction with blood proteins. ACS nano 6, 9485-9495.

Mahmoudi, M., Kalhor, H.R., Laurent, S., Lynch, I., 2013. Protein fibrillation and nanoparticle interactions: opportunities and challenges. Nanoscale 5, 2570-2588.

Mariam, J., Sivakami, S., Dongre, P., 2017. Elucidation of structural and functional properties of albumin bound to gold nanoparticles. Journal of Biomolecular Structure and Dynamics 35, 368-379.

Medhat, A., Mansour, S., El-Sonbaty, S., Kandil, E., Mahmoud, M., 2017. Evaluation of the antitumor activity of platinum nanoparticles in the treatment of hepatocellular carcinoma induced in rats. Tumor Biology 39, 1010428317717259.

Micsonai, A., Wien, F., Bulyáki, É., Kun, J., Moussong, E., Lee, Y.-H., Goto, Y., Réfrégiers, M., Kardos, J., 2018. BeStSel: A web server for accurate protein secondary structure prediction and fold recognition from the circular dichroism spectra. Nucleic acids research 46, W315-W322.

Micsonai, A., Wien, F., Kernya, L., Lee, Y.-H., Goto, Y., Réfrégiers, M., Kardos, J., 2015. Accurate secondary structure prediction and fold recognition for circular

487 dichroism spectroscopy. Proceedings of the National Academy of Sciences 112, E3095-
488 E3103.
489 Moores, A., Goettmann, F., 2006. The plasmon band in noble metal nanoparticles: an
490 introduction to theory and applications. New Journal of Chemistry 30, 1121-1132.
491 Mu, Q., Jiang, G., Chen, L., Zhou, H., Fourches, D., Tropsha, A., Yan, B., 2014.
492 Chemical basis of interactions between engineered nanoparticles and biological systems.
493 Chemical reviews 114, 7740-7781.
494 Pelaz, B., del Pino, P., Maffre, P., Hartmann, R., Gallego, M., Rivera-Fernandez, S., de
495 la Fuente, J.M., Nienhaus, G.U., Parak, W.J., 2015. Surface functionalization of
496 nanoparticles with polyethylene glycol: effects on protein adsorption and cellular uptake.
497 ACS nano 9, 6996-7008.
498 Porcel, E., Li, S., Usami, N., Remita, H., Furusawa, Y., Kobayashi, K., Le Sech, C.,
499 Lacombe, S., 2012. Nano-Sensitization under gamma rays and fast ion radiation,
500 Journal of Physics: Conference Series. IOP Publishing, p. 012006.
501 Porcel, E., Liehn, S., Remita, H., Usami, N., Kobayashi, K., Furusawa, Y., Le Sech, C.,
502 Lacombe, S., 2010. Platinum nanoparticles: a promising material for future cancer
503 therapy? Nanotechnology 21, 085103.
504 Prasanth, S., RitheshRaj, D., Vineeshkumar, T., Sudarsanakumar, C., 2018.
505 Spectroscopic exploration of interaction between PEG-functionalized Ag2S
506 nanoparticles with bovine serum albumin. Chemical Physics Letters 700, 15-21.
507 Rosenberg, B., Vancamp, L., Trosko, J.E., MANSOUR, V.H., 1969. Platinum
508 compounds: a new class of potent antitumour agents. Nature 222, 385.
509 Salado-Leza, D., Porcel, E., Yang, X., Štefančíková, L., Bolsa-Ferruz, M., Savina, F.,
510 Dragoe, D., Guerquin-Kern, J.-L., Wu, T.-D., Hirayama, R., 2020. Green One-Step
511 Synthesis of Medical Nanoagents for Advanced Radiation Therapy. Nanotechnology,
512 Science and Applications 13, 61.
513 Salado-Leza, D., Traore, A., Porcel, E., Dragoe, D., Muñoz, A., Remita, H., García, G.,
514 Lacombe, S., 2019. Radio-enhancing properties of bimetallic Au: Pt nanoparticles:
515 experimental and theoretical evidence. International Journal of Molecular Sciences 20,
516 5648.
517 Sanchez-Guzman, D., Giraudon--Colas, G.l., Marichal, L., Boulard, Y., Wien, F.,
518 Degrouard, J., Baeza-Squiban, A., Pin, S., Renault, J.P., Devineau, S., 2020. In situ
519 analysis of weakly bound proteins reveals molecular basis of soft corona formation.
520 ACS nano 14, 9073-9088.

521 Saptarshi, S.R., Duschl, A., Lopata, A.L., 2013. Interaction of nanoparticles with
522 proteins: relation to bio-reactivity of the nanoparticle. Journal of nanobiotechnology 11,
523 26.
524 Satzer, P., Svec, F., Sekot, G., Jungbauer, A., 2016. Protein adsorption onto
525 nanoparticles induces conformational changes: particle size dependency, kinetics, and
526 mechanisms. Engineering in life sciences 16, 238-246.
527 Schlathölter, T., Eustache, P., Porcel, E., Salado, D., Stefancikova, L., Tillement, O.,
528 Lux, F., Mowat, P., Biegun, A.K., Van Goethem, M.-J., 2016. Improving proton therapy
529 by metal-containing nanoparticles: nanoscale insights. International journal of
530 nanomedicine 11, 1549.
531 Senske, M., Törk, L., Born, B., Havenith, M., Herrmann, C., Ebbinghaus, S., 2014.
532 Protein stabilization by macromolecular crowding through enthalpy rather than entropy.
533 Journal of the American Chemical Society 136, 9036-9041.
534 Shaw, A.K., Pal, S.K., 2008. Spectroscopic studies on the effect of temperature on pH-
535 induced folded states of human serum albumin. Journal of Photochemistry and
536 Photobiology B: Biology 90, 69-77.
537 Shemetov, A.A., Nabiev, I., Sukhanova, A., 2012. Molecular interaction of proteins and
538 peptides with nanoparticles. ACS nano 6, 4585-4602.
539 Srinivasan, M., Rajabi, M., Mousa, S.A., 2015. Multifunctional Nanomaterials and
540 Their Applications in Drug Delivery and Cancer Therapy. Nanomaterials-Basel 5, 1690-
541 1703.
542 Suk, J.S., Xu, Q., Kim, N., Hanes, J., Ensign, L.M., 2016. PEGylation as a strategy for
543 improving nanoparticle-based drug and gene delivery. Advanced drug delivery reviews
544 99, 28-51.
545 Takano, Y., Kusaka, A., Nakamura, H., 2016. Density functional study of molecular
546 interactions in secondary structures of proteins. Biophysics and physicobiology 13, 27-
547 35.
548 Uttayarat, P., Eamsiri, J., Tangthong, T., Suwanmala, P., 2015. Radiolytic synthesis of
549 colloidal silver nanoparticles for antibacterial wound dressings. Advances in Materials
550 Science and Engineering 2015.
551 Wallace, B.A., Janes, R.W., 2010. Synchrotron radiation circular dichroism (SRCD)
552 spectroscopy: an enhanced method for examining protein conformations and protein
553 interactions. Biochemical Society Transactions 38, 861-873.

Wang, C.-L., Hsao, B.-J., Lai, S.-F., Chen, W.-C., Chen, H.-H., Chen, Y.-Y., Chien, C.-C., Cai, X., Kempson, I.M., Hwu, Y., 2011. One-pot synthesis of AuPt alloyed nanoparticles by intense x-ray irradiation. Nanotechnology 22, 065605.

Wang, P., Wang, X., Wang, L., Hou, X., Liu, W., Chen, C., 2015. Interaction of gold nanoparticles with proteins and cells. Science and technology of advanced materials 16, 034610.

Wien, F., Wallace, B., 2005. Calcium fluoride micro cells for synchrotron radiation circular dichroism spectroscopy. Applied spectroscopy 59, 1109-1113.

Yang, X., Bolsa-Ferruz, M., Marichal, L., Porcel, E., Salado-Leza, D., Lux, F., Tillement, O., Renault, J.-P., Pin, S., Wien, F., 2020a. Human serum albumin in the presence of AGuIX nanoagents: Structure stabilisation without direct interaction. International journal of molecular sciences 21, 4673.

Yang, X., Salado-Leza, D., Porcel, E., González-Vargas, C.R., Savina, F., Dragoe, D., Remita, H., Lacombe, S., 2020b. A facile one-pot synthesis of versatile PEGylated platinum nanoflowers and their application in radiation therapy. International journal of molecular sciences 21, 1619.

Yang, X., Salado-Leza, D., Porcel, E., González Vargas, C.R., Savina, F., Dragoe, D., Remita, H., Lacombe, S., 2020c. A Facile One-Pot Synthesis of Versatile PEGylated Platinum Nanoflowers and Their Application in Radiation Therapy. International Journal of Molecular Sciences 21, 1619.

Captions to Figures

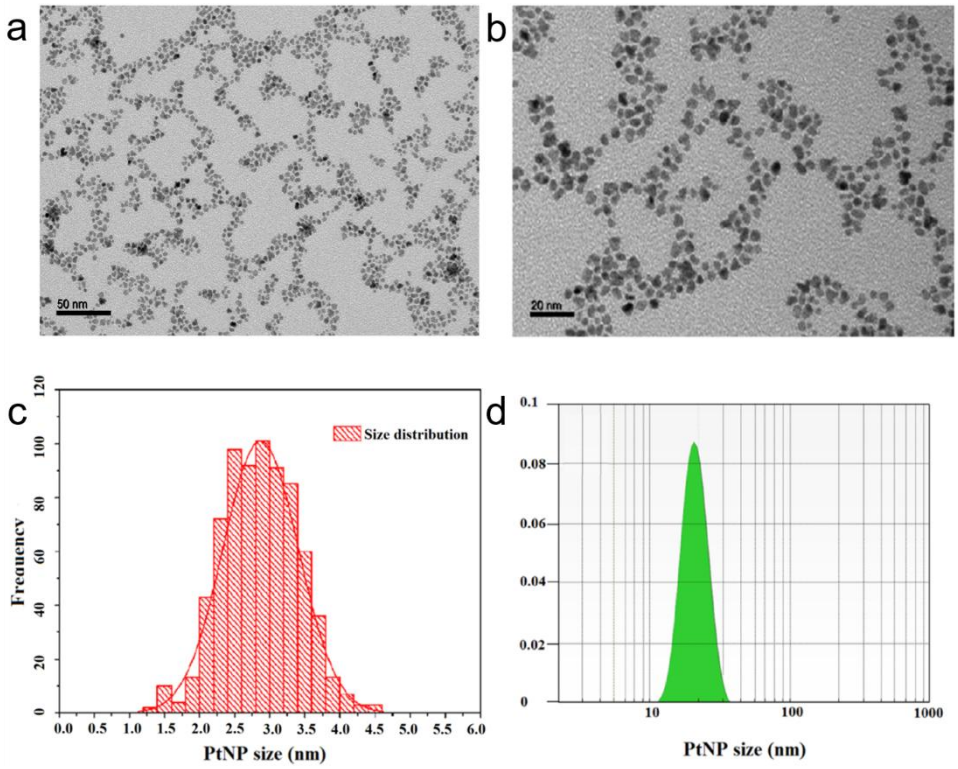

583

584 **Figure 1** (a) TEM image and (b) HRTEM images of Pt NPs; (c) TEM size distribution

585 histogram of Pt NPs; (d) DLS size distribution by intensity of Pt NPs;

586 .

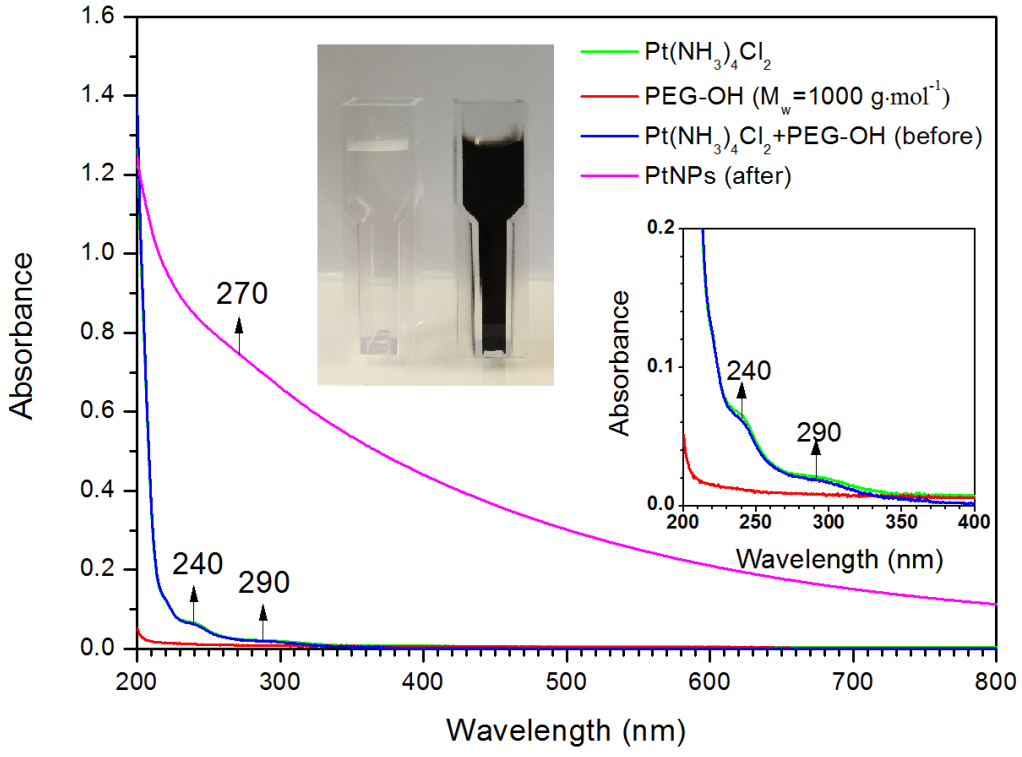

587

588 **Figure 2** UV-vis absorption spectra of $Pt(NH_3)_4Cl_2$ (green line) solution (10^{-3} mol.L^{-1}),
589 PEG-OH (red line) solution (10^{-1} mol.L^{-1}), and diluted Pt containing solutions (10^{-3}
590 mol.L^{-1}) before (blue line) and after (pink line) irradiation (optical path = 2 mm). Inset
591 is the absorption spectra of samples in a wavelength range from 200 to 400 nm.

592

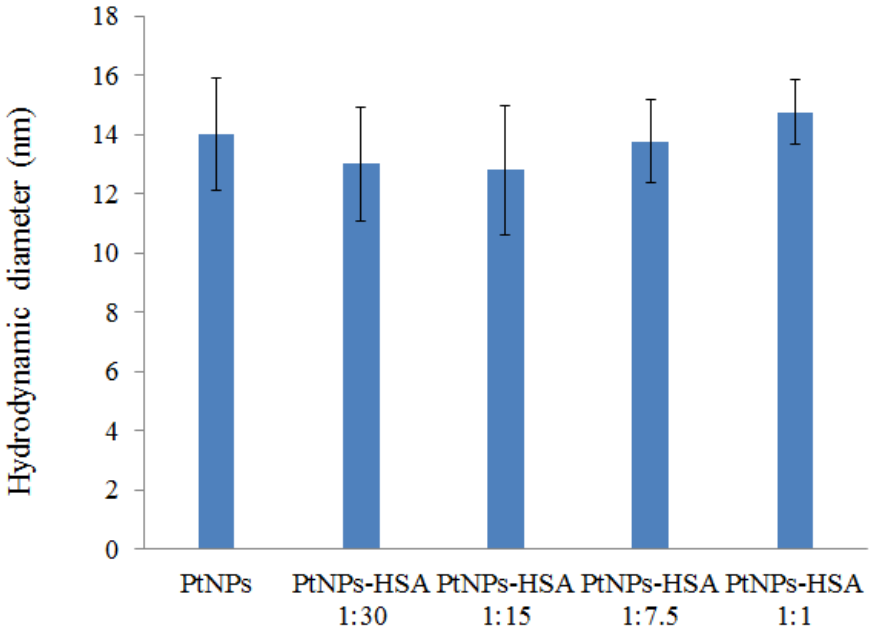

593

594 **Figure 3** Hydrodynamic diameter of Pt NPs and Pt NPs at different Pt NPs-HSA ratios
595 (from 1:30 to 1:1) at pH 7.4, 37°C.

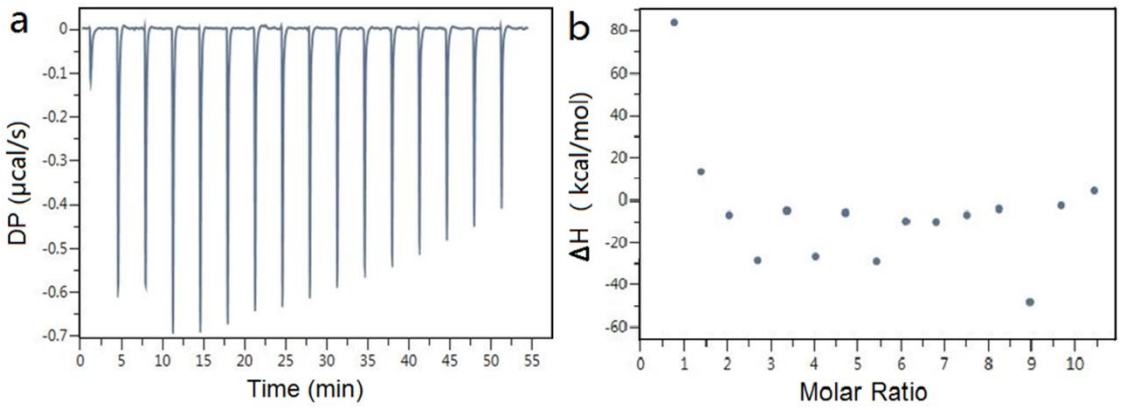

596

597

598 **Figure 4.** Isothermal titration calorimetry (ITC) plots of differential power throughout

599 the titration (a), integrated heat as a function of the mole ratio of Pt NPs-HSA (b).

600

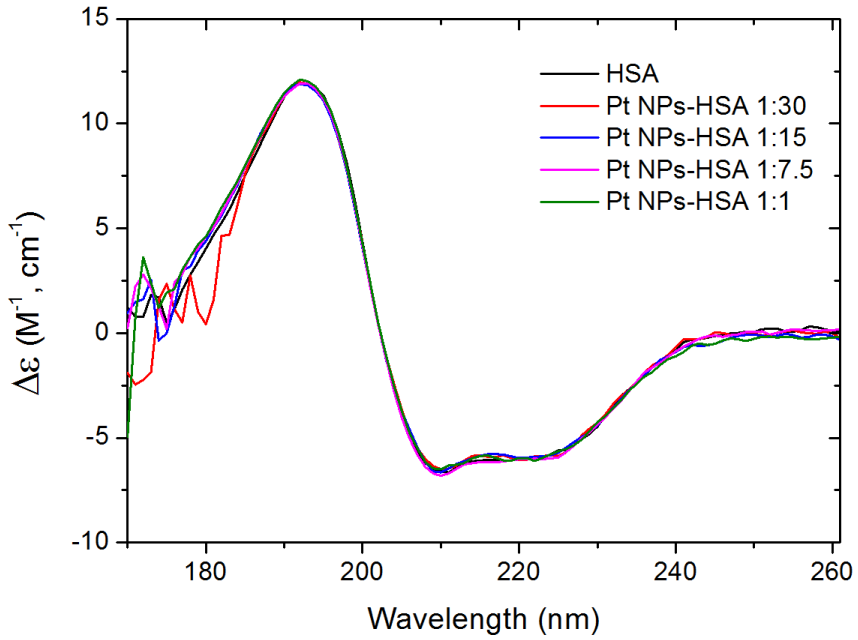

601

602 **Figure 5** SRCD spectra of HSA alone and Pt NPs-HSA at NPs:HSA molar ratios of

603 1:30, 1:15 and 1:7.5 and 1:1, respectively at pH=7.4, 37°C.

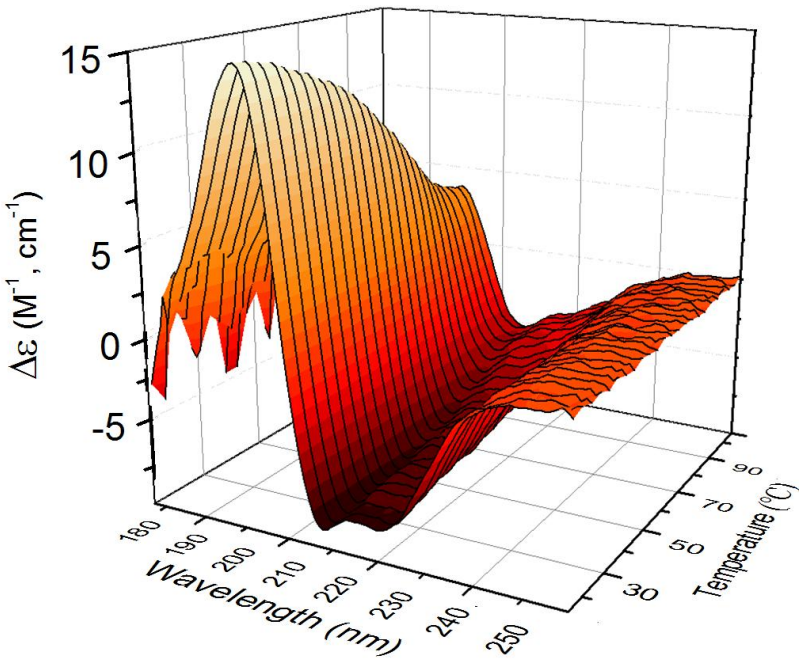

604

Figure 6 Temperature scans of Pt NPs:HSA=1:7.5 with steps of 3°C (from 26°C to 95°C).

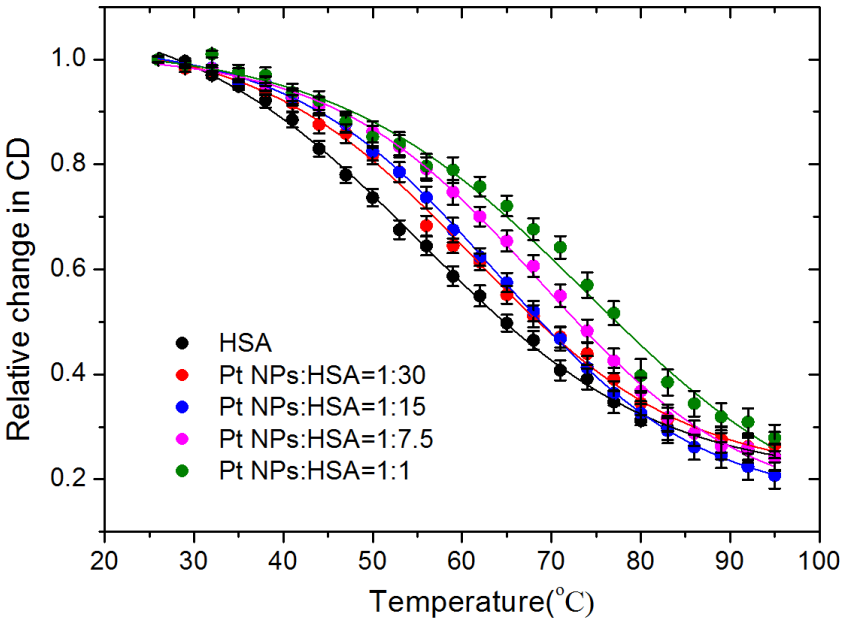

Figure 7 Thermal denaturation curves of pure HSA and the Pt NPs-HSA complex at different ratios (1:30, 1:15, 1:7.5, and 1:1) monitored at 192nm.

Table 1. Values of the melting temperatures Tm, enthalpy variations ΔH° and entropy variations ΔS° for HSA and Pt NPs-HSA at different concentrations (ratios from 1:30 to 1:1) monitored at 192 nm.

Sample	Tm,℃	ΔH°, kJ·mol^{-1}	ΔS°, kJ·mol^{-1}·K^{-1}
HSA	56±0.3	87.3±1.9	0.26±0.006
Pt NPs-HSA 1:30	61±0.3	89.5±1.3	0.27±0.004
Pt NPs-HSA 1:15	64±0.4	92.8±2.0	0.27±0.006
Pt NPs-HSA 1:7.5	69±0.4	101.3±4.2	0.28±0.010
Pt NPs-HSA 1:1	74±0.4	116.4±4.5	0.35±0.014

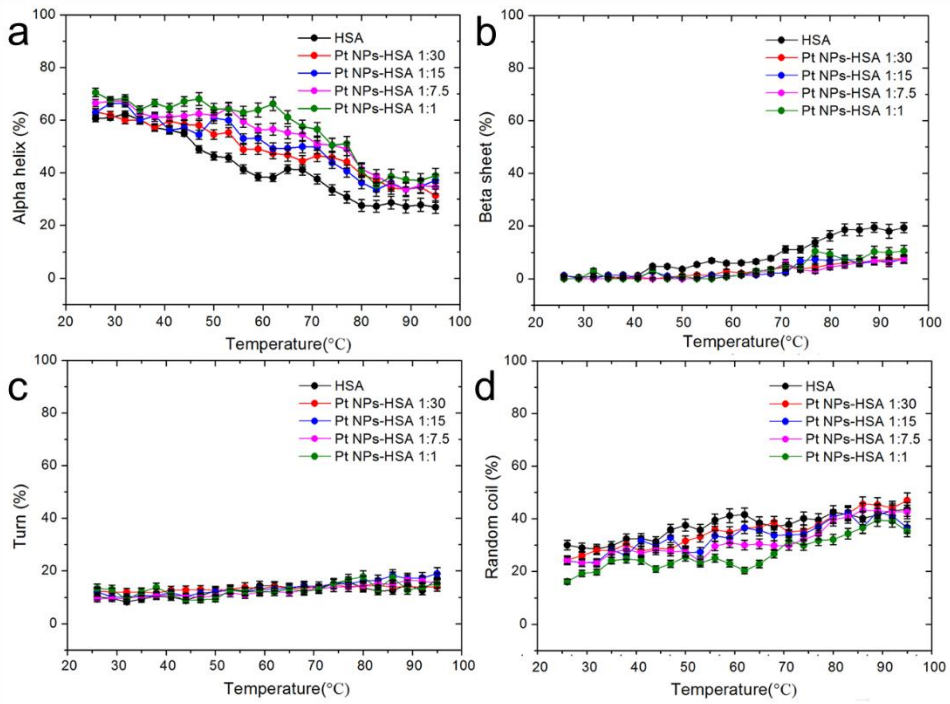

614

615 **Figure 8** Contribution of the protein conformations: alpha-helix (a), beta sheet (b), turns
616 (c), and random coil (d), in the structure of HSA at different temperatures (from 26°C to
617 95°C), in the case of pure HSA and Pt NPs-HSA complex at different ratios (1:30, 1:15,
618 1:7.5, 1:1).

619